Coulomb-induced asymmetry on photoelectron momentum distributions in orthogonal two-color laser fields

Rui-Hua Xu [1], Ying-Kui Zhao,[1,*] Yan-Jun Chen,[2] and Li-Bin Fu [3,†]

[1]*Institute of Applied Physics and Computational Mathematics, Beijing 100094, China*
[2]*College of Physics and Information Technology, Shaan'xi Normal University, Xi'an 710119, China*
[3]*Graduate School, China Academy of Engineering Physics, Beijing 100193, China*

By numerically solving the time-dependent Schrödinger equation, we study the ionization of helium atoms with different forms of the atomic potential, including the soft-core potential, the model potential, and the short-range potential, in orthogonally polarized two-color laser fields. We show that in the case of the long-range atomic potentials (the soft-core potential and the model potential), the photoelectron momentum distributions exhibit asymmetric structures, while for the short-range potential, they present nearly symmetric structures. Besides, the asymmetric structures are sensitive to the specific forms of the atomic potential. We find that the asymmetric structures are more pronounced for the lower laser intensity and/or the shorter laser wavelength. Our results may provide a reference for further analytical studies of strong-field ionization of complex atoms and molecules, where the Coulomb effects are included for quantitative descriptions.

I. INTRODUCTION

The interaction between isolated atoms or molecules and intense laser fields has led to highly nonlinear phenomena [1,2], including the above-threshold ionization [3–6], high-order harmonic generation [6–8], nonsequential double ionization [9–11], and attosecond physics [12,13]. In terms of the theoretical aspect, the three-step recollision model [14,15] and the strong field approximation (SFA) [1,6,16–19] have extensive records of qualitative or semiquantitative success in conforming to the experimental results of some phenomena in strong-field physics. Both in the three-step recollision model and SFA, ionized electrons can be treated as free particles moving in the electric field without the Coulomb interaction. However, the important roles of the Coulomb effects have been discovered in various phenomena, such as the generation of the near- or below-threshold harmonics [20–22], the survival of neutral atoms with creating Rydberg atoms [23], the attosecond measurement techniques [12,24–27], and the quantum interference patterns in the photoelectron momentum distributions (PMDs) [28,29].

Very recently, the Coulomb effects on the final PMDs with a classical or semiclassical trajectory Monte Carlo model and the SFA theory have been explored in the orthogonally polarized two-color (OTC) laser fields [30–33]. The OTC laser fields [34], composed of a fundamental laser field and its phase-locked orthogonally polarized second-order harmonic field, have been widely used to study the atomic ionization, since they enable us to control the photoelectron in both time and space [30–41]. For example,

the OTC laser fields were exploited to generate a single attosecond pulse [35,36], switch short and long quantum trajectories [37], control interference fringes in the photoelectron momentum spectra [31,38,39], probe the time delay of photoelectron emission [40], and investigate the ionization time [41].

In this work, by numerically solving the time-dependent Schrödinger equation (TDSE), we investigate the Coulomb-induced asymmetry in the PMDs in the polarization direction of the second-order harmonic laser field for the helium (He) atoms driven by the OTC laser fields. The Coulomb effects are fully considered both during and after the ionization processes. In addition, it is well known that several specific forms were proposed for the Coulomb potential of real atoms and different forms may have different effects on the electron dynamics. Therefore, here we consider three different forms of the atomic potential, namely the soft-core potential [42], the model potential [43], and the short-range potential. In the case of the long-range atomic potentials (the soft-core and the model potentials), the PMDs present asymmetric structures, while for the short-range Coulomb potential, the PMDs exhibit approximately symmetric structures. Also, we show that the asymmetric structures are sensitive to the specific forms of the long-range atomic potential. Moreover, the asymmetric structures are more pronounced at the lower laser intensity and/or the shorter wavelength.

II. MODEL

In what follows, to explore the Coulomb-induced asymmetry in the PMDs, we consider two long-range potentials (the model potential V_{model} and the soft-core potential V_{soft}) and a short-range potential V_{short} [see Fig. 1(a)],

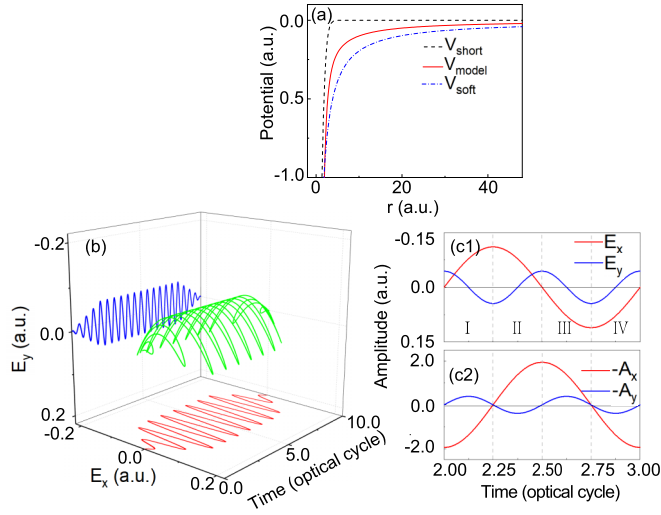*zhao_yingkui@iapcm.ac.cn
†lbfu@gscaep.ac.cn

FIG. 1. (a) Three typical forms of the atomic potential [see Eqs. (1a)–(1c)]: the short-range potential V_{short} (dashed black), the model potential V_{model} (solid red), and the soft-core potential V_{soft} (dash-dotted blue). (b) Schematic diagram of the electric fields of the OTC laser fields [see Eq. (2)]. Here, the peak intensity is 5×10^{14} W/cm² and the carrier frequency is 0.057 a.u.. A trapezoidal pulse envelope is used with a total duration of 10 optical cycles of the fundamental field, switched on and off linearly over two cycles. The total electric field is plotted in green, while the fundamental field and its second-order harmonic field are shown as red and blue lines, respectively. (c1) Amplitude of the fundamental (red) and the second harmonic (blue) fields, and (c2) the corresponding drift momenta caused by the laser fields, $p_x(t) = -A_x(t)$ and $p_y(t) = -A_y(t)$, within one optical cycle of the fundamental field. Four subcycles, I, II, III, and IV are marked in (c1).

given by

$$V_{\text{model}}(r) = -\frac{Z_c + a_1 e^{-a_2 r} + a_3 r e^{-a_4 r} + a_5 e^{-a_6 r}}{r}, \quad (1a)$$

$$V_{\text{soft}}(r) = -\frac{\beta}{\sqrt{r^2 + 0.5}}, \quad (1b)$$

$$V_{\text{short}}(r) = -\frac{\alpha}{\sqrt{r^2 + 0.5}} e^{-0.15 r^2}. \quad (1c)$$

For each potential, all parameters are adjusted such that the eigenenergy of the ground state is -0.9 a.u., which corresponds to the empirical ionization potential of helium. Here, the parameters of the model potential [Eq. (1a)] are $Z_c = 1.0$, $a_1 = 1.231$, $a_2 = 0.662$, $a_3 = -1.325$, $a_4 = 1.236$, $a_5 = -0.231$, and $a_6 = 0.480$. For the soft-core potential [Eq. (1b)] and the short-range potential [Eq. (1c)], the parameters are set to $\beta = 1.961$ and $\alpha = 2.405$, respectively.

In our simulations, a pair of orthogonally polarized two-color laser fields composed of an x-polarized fundamental field and a y-polarized second harmonic field is used [see Fig. 1(b)]. The electric field of the OTC laser fields can be described by

$$\vec{E}(t) = E_0 f(t)[\sin(\omega_0 t)\vec{e}_x + \varepsilon \sin(2\omega_0 t + \phi)\vec{e}_y], \quad (2)$$

where $E_0 = \sqrt{I_0/(1 + \varepsilon^2)}$ is the electric field peak amplitude with I_0 as the peak laser intensity, $f(t)$ is the envelope, ω_0

is the carrier frequency of the fundamental laser field, and $\vec{e}_x$ and $\vec{e}_y$ are the unit vectors along the x and y axes, respectively. Here the relative phase of the OTC laser fields is set to $\phi = \pi/2$. In our calculations, we use $\varepsilon = 0.5$, such that the intensity of the second-order harmonic field is much weaker than that of the fundamental one. As a consequence, the atomic ionization rate is mainly determined by the fundamental field, while the additional second-order harmonic field mildly controls the dynamics of the electron wave packets in the two-dimensional polarization plane (xy plane). According to the three-step recollision model [14,15], without considering the Coulomb potential, the final momenta of electrons ionized at t_0 can be estimated by $\vec{p} = -\vec{A}(t_0)$, where $\vec{A}(t)$ is the vector potential of the laser field. Hence, as plotted in Figs. 1(c1) and 1(c2), photoelectrons ionized at different quarter optical cycles will be launched into different quadrants in the final PMDs. In other words, photoelectrons ionized in the first (I) and the third (III) quarters of the same optical cycle are mapped into the second and the first quadrants with positive momentum along the y direction ($p_y > 0$), while photoelectrons ionized in the second (II) and the fourth (IV) quarters of that optical cycle are mapped into the fourth and the third quadrants with $p_y < 0$. Accordingly, the OTC laser fields can steer the photoelectron in both time and space, allowing us to resolve and control the ultrafast electron dynamics, as compared to the case of parallel polarized two-color laser fields, and the OTC laser fields have been extensively used to probe and control many fascinating phenomena [30–41].

III. NUMERICAL METHOD

In this work, we solve the three-dimensional TDSE of an atom with different forms of the atomic potential driven by the OTC laser fields. The TDSE can be written as (in atomic units)

$$i\frac{\partial}{\partial t}\Psi(\vec{r}, t) = \hat{H}\Psi(\vec{r}, t) = [\hat{H}_0 + \vec{r} \cdot \vec{E}(t)]\Psi(\vec{r}, t), \quad (3)$$

where $\hat{H}_0 = \vec{p}^2/2 + V(\vec{r})$ is the atomic Hamiltonian with $V(\vec{r})$ as the atomic potential. The TDSE is numerically solved using the generalized pseudospectral method [44] in spherical coordinates. The time step is $\Delta t = 0.1$ a.u., and the cutoff of radius and the angular momentum quantum number are set to $R_{\text{max}} = 200$ a.u. and $l_{\text{max}} = 179$, respectively.

In order to eliminate the reflection of the electron wave packet from the boundary and obtain the wave function in the momentum space, the coordinate space is split into the inner and outer regions at a given time t_i [45,46]:

$$\Psi(\vec{r}, t_i) = \Psi_{\text{in}}(\vec{r}, t_i) + \Psi_{\text{out}}(\vec{r}, t_i). \quad (4)$$

Here the wave functions in the outer and inner regions are given by $\Psi_{\text{out}}(\vec{r}, t_i) = F_s(r)\Psi(\vec{r}, t_i)$ and $\Psi_{\text{in}}(\vec{r}, t_i) = [1 - F_s(r)]\Psi(\vec{r}, t_i)$, respectively, where $F_s(r) = 1/\{1 + \exp[-(r - R_c)/\Delta]\}$ is a split function [45,46]. In the simulations, the critical boundary and the width of the crossover region are set to $R_c = 150$ a.u. and $\Delta = 5$ a.u., respectively.

The wave function in the outer region Ψ_{out} is propagated analytically under the Coulomb-Volkov Hamiltonian [32,46–53], which can reduce the computational loads of nu-
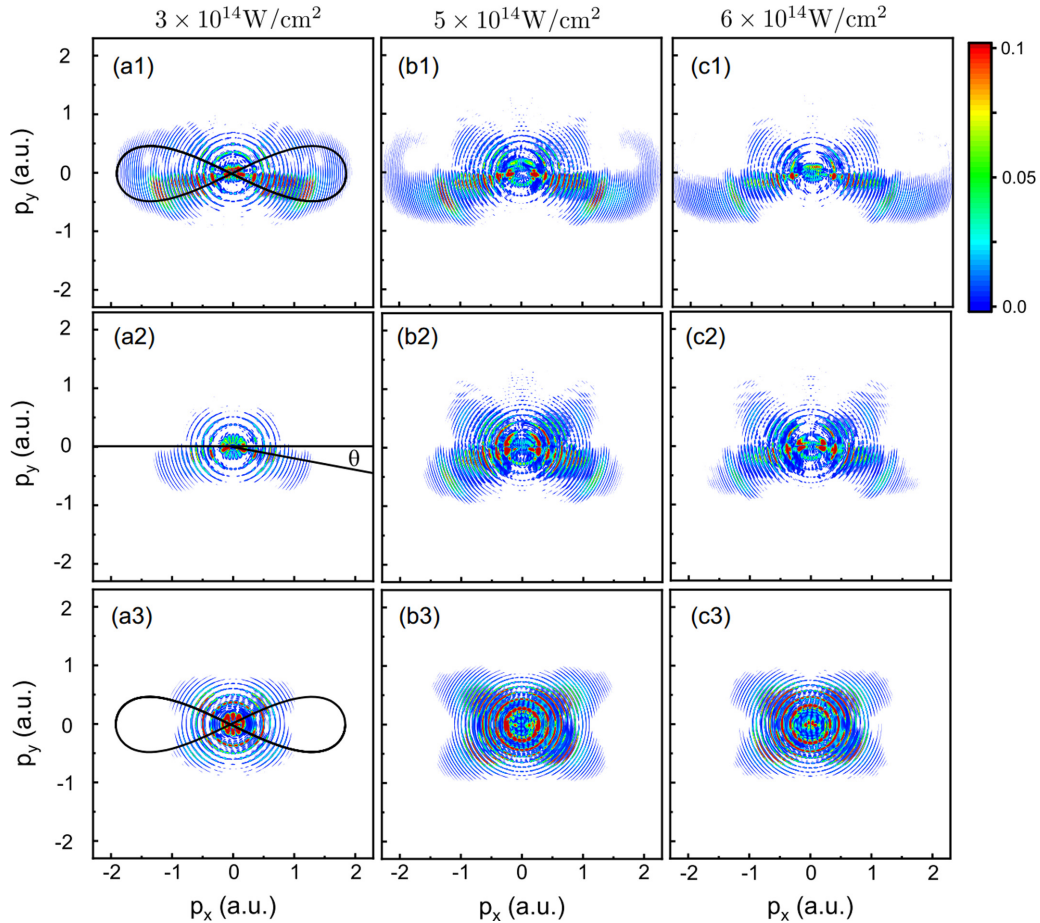
FIG. 2. Photoelectron momentum distributions in the xy polarization plane with $p_z = 0$ at different laser intensities for the soft-core potential (top row), the model potential (middle row), and the short-range potential (bottom row). The laser wavelength is 800 nm. The black curves in (a1) and (a3) denote the field-driven photoelectron momenta $\vec{p} = -\vec{A}(t)$ within one optical cycle of the fundamental field. Panels in the column from left to right corresponds to the intensities of 3×10^{14}, 5×10^{14}, and 6×10^{14} W/cm^2, respectively. The tilt angle θ is the angle between the p_x axis and the most probable direction of distribution, as marked in panel (a2).

merically tough problems. Specifically, we expand the wave function in the outer region at time t_i in the basis of Coulomb-Volkov states $\Psi_{\vec{p}}^{CV}(t_i)$, and the projection coefficients are given by

$$C(\vec{p}, t_i) = \int [\Psi_{\vec{p}}^{CV}(t_i)]^* \Psi_{\text{out}}(t_i) d^3\vec{r}. \qquad (5)$$

Then we propagate Ψ_{out} from t_i to the end of the laser pulse (t_f) under the Volkov propagator [45]

$$\hat{U}_V(t_f, t_i) = \exp\left\{ -\frac{i}{2} \int_{t_i}^{t_f} \left[\vec{p} + \vec{A}(t') \right]^2 dt' \right\}. \qquad (6)$$

Accordingly, the photoelectron momentum distributions at t_f can be written as [45]

$$|\Phi(\vec{p}, t_f)|^2 = \left| \sum_i \hat{U}_V(t_f, t_i) C(\vec{p}, t_i) \right|^2. \qquad (7)$$

In the case of SFA [1,6,16–19], after the tunneling process, the electron is treated as a free particle moving in the external field with neglecting the Coulomb effects. As a consequence, the dynamics of the ionized electron can be described by the

evolution of the Volkov states propagating under the Volkov propagator. On the other hand, a modified SFA theory was proposed to describe the ionized electron by replacing the Volkov states with Coulomb-Volkov states [54,55]. As noted, the Coulomb effects are considered in the modified SFA theory, since Coulomb-Volkov states are instantaneous eigenstates of the electron interacting with the laser field and the Coulomb potential. Similarly, the Coulomb effects are also considered in the outer region in the method presented here.

IV. COULOMB-INDUCED ASYMMETRY ON PMDS

With the help of the numerical method introduced in Sec. III, we plot the two-dimensional PMDs ($p_z = 0$) of helium atom with different potentials driven by the two-color fields in Fig. 2. In the case of the soft-core potential [see Figs. 2(a1)–2(c1)] and the model potential [see Figs. 2(a2)–2(c2)], the two-dimensional PMDs exhibit butterfly-like structures with up-down asymmetries. The momentum distributions in these cases have higher probabilities in the lower half-plane ($p_y < 0$) than in the upper half-plane ($p_y > 0$). To explore the effects of the atomic potential on the asymmetric

structures, for comparison, we plot the results of the short-range potential V_{short} in Figs. 2(a3)–2(c3). Obviously, the PMDs present the X-shaped structures with nearly up-down symmetries. In this case, the absolute value of the potential rapidly decays to 0 [see Fig. 1(a)], such that the dynamics of the ionized electron is hardly affected by this short-range potential. Accordingly, the field-driven momenta of photo-electrons nearly follow the relation $\vec{p} = -\vec{A}(t)$ [see black lines in Fig. 2(a3)], ignoring the effect of the atomic potential, resulting in the up-down symmetric X-shaped structures in the PMDs [30,32]. In contrast, the results in the case of the soft-core potential [see Figs. 2(a1)–2(c1)] and the model potential [see Figs. 2(a2)–2(c2)] indicate that asymmetric structures are ascribed to the long-range effect of the atomic potential on the photoelectron dynamics, which is consistent with the interpretations based on the results of a classical trajectory Monte Carlo (CTMC) model [30,31] and the SFA [32]. They [30–32] suggest that the Coulomb attraction decreases the contribution of photoelectrons born in the first (I) and the third (III) quarters of the optical cycle [see Fig. 1(c1)], while in the second (II) and the fourth (IV) quarters of the optical cycle, the Coulomb attraction increases the contribution of photoelectrons by affecting the recollision processes.

Furthermore, the asymmetric structures depend not only on the long-range potential, but also on its specific forms. As shown in Figs. 1(a), the model potential has a singularity at $r = 0$ a.u. and it changes sharply near the parent ion core, while the soft-core potential changes quite slowly at $r \simeq 0$ a.u. In addition, the absolute value of the soft-core potential is always larger than that of the model potential. This means the effect of the soft-core potential on the photoelectron dynamics is always stronger, resulting in the more pronounced asymmetric structures [see Figs. 2(a1)–2(c1) and 2(a2)–2(c2)].

In addition to the atomic potential, the laser fields act on the behavior of photoelectrons as well. Figure 2 depicts the laser intensity dependence of the PMDs for three potentials. As can be seen from three panels in the same row, with the increase of the laser intensity, the up-down asymmetry becomes weaker. Specifically, when the laser field is very strong, the atomic potential is sufficiently small and negligible compared to it. In this case, the long-range potential can be treated as a short-range potential, so the butterfly-like structure tends to the X-shaped structures; that is, the up-down asymmetry is weak. Furthermore, Fig. 3 shows the PMDs for different laser wavelengths. The up-down asymmetry becomes weaker for the longer wavelength (also see the three panels in the middle column in Fig. 2, corresponding to the case of 800 nm). To our knowledge, the recollision processes are also sensitive to the laser intensity and wavelength [56–60]. The dependence of the laser intensity and wavelength on the Coulomb-induced asymmetry presented here is similar to the dependence on the recollision processes.

In the presence of the OTC field, in order to recollide, electrons must be emitted at an initial transverse velocity v_{y_0}, which should offset the drift velocity v_d along the polarization direction of the second harmonic field [56–60], since the second-order harmonic field tends to pull the electrons away transversely and resist the recollision. As predicted by the SFA [18], the initial transverse velocity satisfies a Gaussian distribution with standard deviation $\sigma = (E_0/\sqrt{2I_p})^{1/2}$, where I_p is
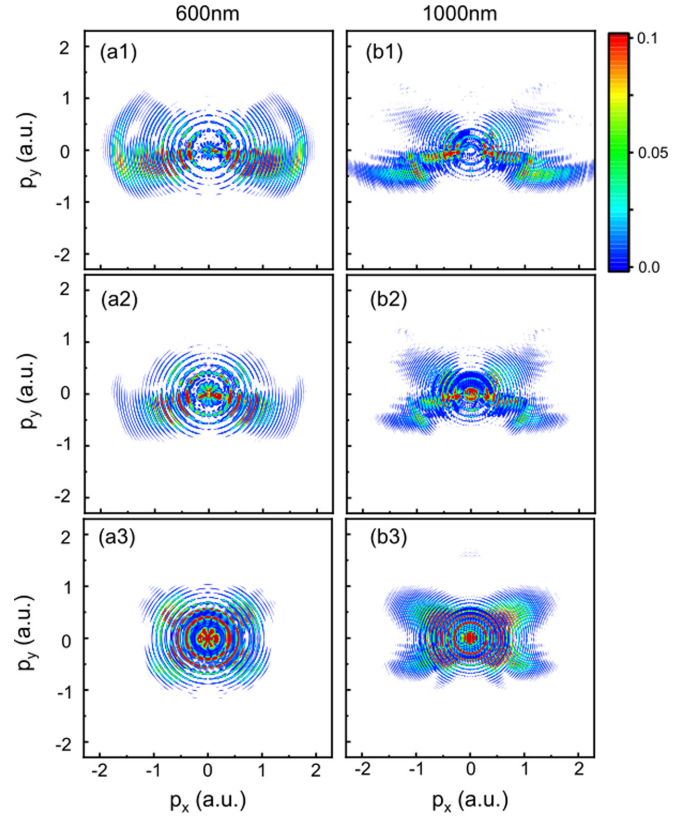

FIG. 3. Photoelectron momentum distributions. The conditions used are the same as the case shown in the middle column in Fig. 2 except that the wavelengths in the left and right columns are 600 and 1000 nm, respectively.

the ionization potential. Moreover, the drift velocity caused by the vector potential of the laser field is $v_d = \varepsilon E_0/2\omega_0$ (atomic units are used) [14,18]. Hence, the probability of generating an electron with $v_{y_0} \simeq -v_d$ can be estimated by the ratio of v_d to σ,

$$R \equiv \frac{v_d}{\sigma} = \frac{\varepsilon E_0 \gamma^{1/2}}{2\omega_0^{3/2}} = \frac{\varepsilon r_q (\omega_0 \gamma)^{1/2}}{2}, \tag{8}$$

where $r_q = E_0/\omega_0^2$ is the quiver amplitude of the electron in the laser field and $\gamma = \omega_0\sqrt{2I_p}/E_0$ is the Keldysh parameter [1]. As we know, a smaller quiver amplitude r_q, which means that electrons oscillate in a region closer to the parent ion, makes the recollision processes more susceptible to occur by the Coulomb attraction. Also, for a smaller Keldysh parameter γ, the recollision processes are more important. Correspondingly, the probability of recollision processes is higher with a smaller ratio R. Note that when the laser intensity E_0 and the carrier frequency ω_0 vary, there is a competition between the Keldysh parameter γ and the quiver amplitude r_q. However, the ratio R is overall positively correlated with E_0/ω_0. Therefore, with a lower intensity E_0 and a higher carrier frequency ω_0, the ratio R is smaller, indicating the recollision process is more important and up-down asymmetry is more pronounced, consistent with the results shown in Figs. 2 and 3.
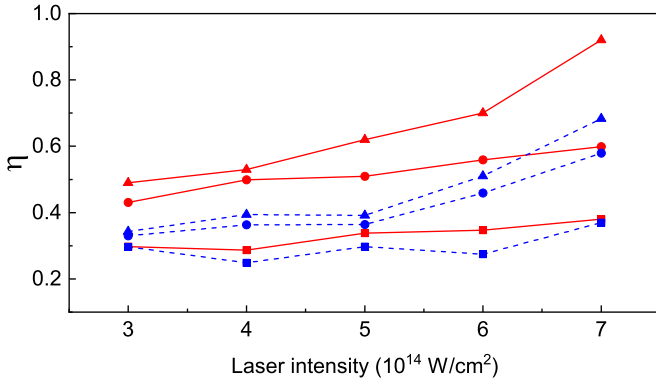
FIG. 4. Up-down symmetry parameter, η as a function of the laser intensity for the soft-core potential (dashed blue lines) and the model potential (solid red lines) with three laser wavelengths: 600 nm (square markers), 800 nm (circle markers), and 1000 nm (triangle markers).

To identify the degree of the up-down symmetry, we introduce a parameter

$$\eta = \frac{\int_{p_y>0, p_z=0} |\Phi(\vec{p}, t_f)|^2 d^3 \vec{p}}{\int_{p_y<0, p_z=0} |\Phi(\vec{p}, t_f)|^2 d^3 \vec{p}}. \qquad (9)$$

Here, $\eta = 1$ corresponds to the up-down symmetric structures in the PMDs, and $\eta > 1$ and $\eta < 1$ represent the higher probabilities in the upper ($p_y > 0$) and lower ($p_y < 0$) half-planes in the PMDs, respectively.

Figure 4 depicts the up-down symmetry parameter η as a function of the laser intensity for the soft-core potential and the model potential with three laser wavelengths, namely 600 nm (square markers), 800 nm (circle markers), and 1000 nm (triangle markers). Here we only consider the cases of the long-range potential, since η in the case of the short-range potential is approximately 1 (see Figs. 2 and 3).

The up-down symmetry parameter, η is always lower than 1, which means the laser parameters used here prefer to induce the photoelectrons with $p_y < 0$. Under the same laser parameters, for the model potential (see the solid red lines in Fig. 4), the degrees of up-down symmetry are always greater than that of the soft-core one (see the dashed blue lines in Fig. 4). Also, η is greater with the increase of the laser intensity and the wavelength. The results show that the behavior of the up-down symmetry parameter is well described by R. To further explore the insight physics of the effects of the atomic potentials on the PMDs, we plot the dependence of ellipticity ε on the tilt angle θ in Fig. 5. Here θ is the angle between the p_x axis and the most probable direction of distribution, as marked in Fig. 2 (a2). If the Coulomb effect is not included, θ is approximately given by

$$\theta \approx \left| \arctan\left(\frac{p_y}{p_x}\right) \right| \approx \left| \arctan\left[\frac{-A_y(t_0)}{-A_x(t_0)}\right] \right|$$
$$= |\arctan[\varepsilon \sin(\omega_0 t_0)]|. \qquad (10)$$

Considering that the electrons are most likely to be ionized at the peak of the external field [$\sin(\omega_0 t_0) = \pm 1$] [2], θ can thus be estimated by $\arctan(\varepsilon)$ with ignoring the Coulomb potential. As shown in Fig. 5, among the three potentials
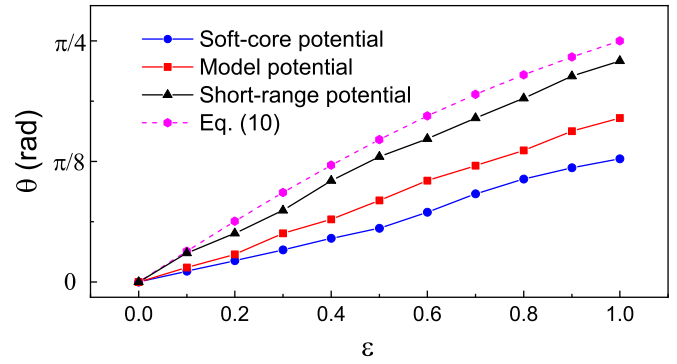

FIG. 5. Tilt angle θ as a function of the laser ellipticity ε for three atomic potentials: the soft-core potential (blue circle), the model potential (red square), and the short-range potential (black triangle). For comparison, the pink hexagon line is the prediction given by Eq. (10). The laser intensity is 5×10^{14} W/cm^2 and the laser wavelength is 800 nm.

used here, the tilt angle θ for the short-range potential has the smallest deviation from the prediction given by Eq. (10), while for the soft-core potential, it has the largest deviations. Note that even the short-range potential, θ still differs from the angle predicted by the Eq. (10), which implies that the short-range potential may play an important role in the ionization processes.

V. CONCLUSION

In summary, we have investigated the Coulomb-induced up-down asymmetry in PMDs of helium atoms driven by a pair of orthogonally polarized two-color laser fields. In our simulations, during and after the ionization processes, the effects of the atomic potential are fully considered. By comparing the results of the long-range and the short-range potentials, we find that the up-down asymmetric structures in PMDs is dominated by long-range effect of the potential. Also, we show that the forms of the long-range atomic potential play an important role in the asymmetric structures by comparing the calculations of the model potential and the soft-core potential. Furthermore, the asymmetric structures become more pronounced for the lower laser intensity and/or the shorter laser wavelength. We also study the dependence of the ellipticity of the OTC laser fields on the up-down asymmetry and find that the atomic potential affects the dynamics of electrons during the ionization process as well. Our results may provide a reference for further analytical studies of strong-field ionization of complex atoms and molecules, where the Coulomb effects are included for quantitative descriptions.

---

[1] L. V. Keldysh, Sov. Phys. JETP **20**, 1307 (1965).

[2] M. V. Ammosov, N. B. Delone, and V. P. Krainov, Sov. Phys. JETP **64**, 1191 (1986).

[3] P. Agostini, F. Fabre, G. Mainfray, G. Petite, and N. K. Rahman, Phys. Rev. Lett. **42**, 1127 (1979).

[4] B. Yang, K. J. Schafer, B. Walker, K. C. Kulander, P. Agostini, and L. F. DiMauro, Phys. Rev. Lett. **71**, 3770 (1993).

[5] G. G. Paulus, W. Nicklich, H. Xu, P. Lambropoulos, and H. Walther, Phys. Rev. Lett. **72**, 2851 (1994).

[6] M. Lewenstein, K. C. Kulander, K. J. Schafer, and P. H. Bucksbaum, Phys. Rev. A **51**, 1495 (1995).

[7] A. McPherson, G. Gibson, H. Jara, U. Johann, T. S. Luk, I. A. McIntyre, K. Boyer, and C. K. Rhodes, JOSA B **4**, 595 (1987).

[8] M. Ferray, A. L'Huillier, X. F. Li, L. A. Lompre, G. Mainfray, and C. Manus, J. Phys. B **21**, L31 (1988).

[9] B. Walker, B. Sheehy, L. F. DiMauro, P. Agostini, K. J. Schafer, and K. C. Kulander, Phys. Rev. Lett. **73**, 1227 (1994).

[10] S. Palaniyappan, A. Di Chiara, E. Chowdhury, A. Falkowski, G. Ongadi, E. L. Huskins, and B. C. Walker, Phys. Rev. Lett. **94**, 243003 (2005).

[11] W. Becker, X. J. Liu, P. J. Ho, and J. H. Eberly, Rev. Mod. Phys. **84**, 1011 (2012).

[12] F. Krausz and M. Ivanov, Rev. Mod. Phys. **81**, 163 (2009).

[13] R. Pazourek, S. Nagele, and J. Burgdörfer, Rev. Mod. Phys. **87**, 765 (2015).

[14] P. B. Corkum, Phys. Rev. Lett. **71**, 1994 (1993).

[15] K. J. Schafer, B. Yang, L. F. DiMauro, and K. C. Kulander, Phys. Rev. Lett. **70**, 1599 (1993).

[16] F. H. M. Faisal, J. Phys. B **6**, L89 (1973).

[17] H. R. Reiss, Phys. Rev. A **22**, 1786 (1980).

[18] M. Y. Ivanov, M. Spanner, and O. Smirnova, J. Mod. Opt. **52**, 165 (2005).

[19] M. Lewenstein, P. Balcou, M. Y. Ivanov, A. L'Huillier, and P. B. Corkum, Phys. Rev. A **49**, 2117 (1994).

[20] H. Soifer, P. Botheron, D. Shafir, A. Diner, O. Raz, B. D. Bruner, Y. Mairesse, B. Pons, and N. Dudovich, Phys. Rev. Lett. **105**, 143904 (2010).

[21] J. A. Hostetter, J. L. Tate, K. J. Schafer, and M. B. Gaarde, Phys. Rev. A **82**, 023401 (2010).

[22] W. H. Xiong, J. W. Geng, J. Y. Tang, L. Y. Peng, and Q. Gong, Phys. Rev. Lett. **112**, 233001 (2014).

[23] K. Y. Huang, Q. Z. Xia, and L. B. Fu, Phys. Rev. A **87**, 033415 (2013).

[24] M. Hentschel, R. Kienberger, C. Spielmann, G. A. Reider, N. Milosevic, T. Brabec, P. Corkum, U. Heinzmann, M. Drescher, and F. Krauzs, Nature (London) **414**, 509 (2001).

[25] P. Eckle, A. N. Pfeiffer, C. Cirelli, A. Staudte, R. D'Örner, H. G. Muller, M. Büttiker, and U. Keller, Science **322**, 1525 (2008).

[26] P. Eckle, M. Smolarski, P. Schlup, J. Biegert, A. Staudte, M. Schöffler, H. G. Muller, R. Dörner, and U. Keller, Nat. Phys. **4**, 565 (2008).

[27] M. Schultze, M. Fieß, N. Karpowicz, J. Gagnon, M. Korbman, M. Hofstetter, S. Neppl, A. L. Cavalieri, Y. Komninos, Th. Mercouris, C. A. Nicolaides, R. Pazourek, S. Nagele, J. Feist, J. Burgdörfer, A. M. Azzeer, R. Ernstorfer, R. Kienberger, U. Kleineberg, E. Goulielmakis *et al.*, Science **328**, 1658 (2010).

[28] D. G. Arbó, K. L. Ishikawa, K. Schiessl, E. Persson, and J. Burgdörfer, Phys. Rev. A **81**, 021403(R) (2010).

[29] J. Kaushal and O. Smirnova, Phys. Rev. A **88**, 013421 (2013).

[30] L. Zhang, X. H. Xie, S. Roither, D. Kartashov, Y. L. Wang, C. L. Wang, M. Schöffler, D. Shafir, P. B. Corkum, A. Baltuška, I. Ivanov, A. Kheifets, X. J. Liu, A. Staudte, and M. Kitzler, Phys. Rev. A **90**, 061401(R) (2014).

[31] M. Li, J. W. Geng, M. M. Liu, X. Zheng, L. Y. Peng, Q. H. Gong, and Y. Q. Liu, Phys. Rev. A **92**, 013416 (2015).

[32] S. G. Yu, Y. L. Wang, X. Y. Lai, Y. Y. Huang, W. Quan, and X. J. Liu, Phys. Rev. A **94**, 033418 (2016).

[33] X. J. Xie, C. Chen, G. G. Xin, J. Liu, and Y. J. Chen, Opt. Express **28**, 33228 (2020).

[34] M. Kitzler and M. Lezius, Phys. Rev. Lett. **95**, 253001 (2005).

[35] C. M. Kim, I. J. Kim, and C. H. Nam, Phys. Rev. A **72**, 033817 (2005).

[36] Y. L. Yu, X. H. Song, Y. X. Fu, R. X. Li, Y. Cheng, and Z. Z. Xu, Opt. Express **16**, 686 (2008).

[37] L. Brugnera, D. J. Hoffmann, T. Siegel, F. Frank, A. Zaïr, J. W. G. Tisch, and J. P. Marangos, Phys. Rev. Lett. **107**, 153902 (2011).

[38] X. Xie, Phys. Rev. Lett. **114**, 173003 (2015).

[39] M. Richter, M. Kunitski, M. Schöffler, T. Jahnke, L. P. H. Schmidt, M. Li, Y. Q. Liu, and R. Dörner, Phys. Rev. Lett. **114**, 143001 (2015).

[40] X. Gong, C. Lin, F. He, Q. Song, K. Lin, Q. Ji, W. Zhang, J. Ma, P. Lu, Y. Liu, H. Zeng, W. Yang, and J. Wu, Phys. Rev. Lett. **118**, 143203 (2017).

[41] J. Tan, Y. Zhou, M. He, Y. Chen, Q. Ke, J. Liang, X. Zhu, M. Li, and P. Lu, Phys. Rev. Lett. **121**, 253203 (2018).

[42] Q. Su and J. H. Eberly, Phys. Rev. A **44**, 5997 (1991).

[43] X. M. Tong and C. D. Lin, J. Phys. B **38**, 2593 (2005).

[44] X. M. Tong and S. I. Chu, Chem. Phys. **217**, 119 (1997).

[45] X. M. Tong, K. Hino, and N. Toshima, Phys. Rev. A **74**, 031405(R) (2006).

[46] X. M. Tong, J. Phys. B **50**, 144004 (2017).

[47] G. Duchateau, E. Cormier, H. Bachau, and R. Gayet, Phys. Rev. A **63**, 053411 (2001).

[48] G. Duchateau, E. Cormier, and R. Gayet, Phys. Rev. A **66**, 023412 (2002).

[49] D. G. Arbó, J. E. Miraglia, M. S. Gravielle, K. Schiessl, E. Persson, and J. Burgdörfer, Phys. Rev. A **77**, 013401 (2008).

[50] L. Y. Peng and Q. Gong, Comput. Phys. Commun. **181**, 2098 (2010).

[51] D. G. Arbó, S. Nagele, X. M. Tong, X. Xie, M. Kitzler, and J. Burgdörfer, Phys. Rev. A **89**, 043414 (2014).

[52] F. H. M. Faisal, Phys. Rev. A **94**, 031401(R) (2016).

[53] J. Cai, Y. J. Chen, Q. Z. Xia, D. F. Ye, J. Liu, and L. B. Fu, Phys. Rev. A **96**, 033413 (2017).

[54] M. Jain and N. Tzoar, Phys. Rev. A **18**, 538 (1978).

[55] P. Cavalieri, G. Ferrante, and C. Leone, J. Phys. B **13**, 4495 (1980).

[56] L. B. Fu, G. G. Xin, D. F. Ye, and J. Liu, Phys. Rev. Lett. **108**, 103601 (2012).

[57] X. Wang and J. H. Eberly, Phys. Rev. Lett. **105**, 083001 (2010).

[58] F. Mauger, C. Chandre, and T. Uzer, Phys. Rev. Lett. **105**, 083002 (2010).

[59] R. Kopold, D. B. Milosevic, and W. Becker, Phys. Rev. Lett. **84**, 3831 (2000).

[60] Y. H. Lai, X. Wang, Y. Li, X. Gong, B. Talbert, C. I. Blaga, P. Agostini, and L. F. DiMauro, Phys. Rev. A **101**, 013405 (2020).